Research Article

Series Resistance Analysis of Passivated Emitter Rear Contact Cells Patterned Using Inkjet Printing

Martha A. T. Lenio,[1] James Howard,[1] Doris (Pei Hsuan) Lu,[1] Fabian Jentschke,[2] Yael Augarten,[1] Alison Lennon,[1] and Stuart R. Wenham[1]

[1] *Electrical Engineering Department, School of Photovoltaic and Renewable Energy Engineering, University of New South Wales, Sydney, NSW 2052, Australia*
[2] *Energy Australia, Sydney, NSW 2001, Australia*

Correspondence should be addressed to Martha A. T. Lenio, m.lenio@student.unsw.edu.au

For higher-efficiency solar cell structures, such as the Passivated Emitter Rear Contact (PERC) cells, to be fabricated in a manufacturing environment, potentially low-cost techniques such as inkjet printing and metal plating are desirable. A common problem that is experienced when fabricating PERC cells is low fill factors due to high series resistance. This paper identifies and attempts to quantify sources of series resistance in inkjet-patterned PERC cells that employ electroless or light-induced nickel-plating techniques followed by copper light-induced plating. Photoluminescence imaging is used to determine locations of series resistance losses in these inkjet-patterned and plated PERC cells.

1. Introduction

As the photovoltaics industry becomes more mature, manufacturers must find new ways of staying competitive. Developing cost-effective ways of fabricating higher-efficiency cell structures that have to date only been realized in a laboratory environment is an option that is being considered by many. An obvious cell structure to attempt to commercialise is the Passivated Emitter Rear Contact (PERC) cell [1, 2].

New patterning methods such as inkjet printing and laser doping [3–5] enable the patterning of dielectric layers for metal contacting and therefore eliminate the need to use techniques such as photolithography which enabled the earlier laboratory implementations of these cells. Metal plating, which has been successfully used for the manufacture of photovoltaic devices in industry [6], is compatible with these patterning methods and consequently presents as a commercially viable metallization method. In addition to enabling the use of less expensive metals like Ni and Cu, metal plating is a self-aligning process thus eliminating the need for the photolithographic lift-off steps which were used

in conjunction with evaporated Ti-Pd-Ag metal contacts. A further advance that is desirable to make PERC cells commercially viable is to reduce the number of high temperature steps [7, 8].

This paper contains an analysis of the series resistance losses of PERC cells that have been fabricated using inkjet printing (IJP) for the patterning steps and self-aligned Ni and Cu plating for the metallization. The fabricated PERC cells were analyzed using photoluminescence (PL) imaging, current-voltage (IV) measurements, and microscopy. Transmission line model (TLM) test structures were fabricated to characterize the metal-silicon interface and estimate the contact resistance associated with both the front and rear metal contacts. The findings of this work show that a decrease in fill factor due to high series resistive losses is a problem with electrolessly plated PERC cells. This is consistent with the findings of other researchers who have seen fill factor losses in their electrolessly plated PERC cells that were formed using laser-fired rear contacts [9]. It was found here that spurious Ni plating on the rear point contacts forms during electroless Ni plating, and this contributes

significantly to the high series resistance and resulting low fill factors of final devices. Poorly adhered front contacts were also an issue with inkjet-printed and electrolessly plated PERC cells. It is shown that use of appropriate plating techniques, such as bias-assisted light induced plating, can help reduce these resistive effects.

2. Experimental Procedure

2.1. Cell and Test Structure Fabrication. Cells and test structures were fabricated on planar, $0.5 \, \Omega \cdot \text{cm}$, p-type, $200 \, \mu\text{m}$ thick, FZ Si wafers. The processing sequence used for the cells is outlined in Table 1. The emitter sheet resistance after processing was $\sim 120 \, \Omega/\square$. Nickel contacts were formed using both electroless plating and bias-assisted LIP. In the latter process, a bias voltage of 0.6 V was applied to the rear Al surface of the devices (this setup can be seen in Figure 1(a)). All Cu plating was performed using noncontact LIP without an applied bias (see Figure 1(b)).

The dimensions of the completed cells are detailed in Table 2. The TLM test structures underwent the same thermal processing as the fabricated cells. The only difference in the fabrication sequence was the inkjet patterning. Instead of forming openings for front finger grids and rear point contacts, TLM contact pads were patterned using the indirect inkjet patterning method [5] for the (front) Ni and (rear) Al contact resistance test structures. For the rear measurements, TLM contact pads of Al were evaporated through a mask which was aligned to the inkjet-patterned openings in the rear SiO_2 dielectric layer.

2.2. Analysis. The series resistance of the final IJP PERC cells was estimated from comparing the light-IV measurements with the Suns-V_{oc} measurements [10]. Photoluminescence (PL) imaging was used to record a spatially resolved image of the voltage across the cells. Two types of PL imaging were used: open-circuit PL and R_s-PL [11, 12]. The contributing components of the series resistance were identified, and each component was calculated using actual dimensions and resistances measured from test structures. Scanning electron microscope (SEM), focused ion beam (FIB), and optical microscopy were used to inspect the quality of the metal contacts and to help determine the underlying causes of the high series resistance problems experienced by IJP PERC cells.

3. Results and Discussion

3.1. Contact Resistance Results. The TLM measurements for the front Ni contacts depended on the plating technique used, with the average specific contact resistivity being $0.07 \pm 0.04 \, \Omega \cdot \text{cm}^2$ and $0.09 \pm 0.02 \, \Omega \cdot \text{cm}^2$ for electroless Ni and bias-assisted LIP Ni contacts, respectively. There were some variations between individual test structures using the same Ni-plating technique, particularly with the electroless Ni-plated cells. Specific contact resistivities as low as $3.5 \times 10^{-5} \, \Omega \cdot \text{cm}^2$ have been reported previously for Ni/Cu-plated fingers [19]. The discrepancy between the resistivity values

could be due to the difficulty experienced in achieving good adhesion between the Ni and Si.

The specific contact resistivity for the Al-Si rear contact TLM test structures was measured to be $0.004 \pm 0.003 \, \Omega \cdot \text{cm}^2$ and $0.028 \pm 0.010 \, \Omega \cdot \text{cm}^2$, before and after electroless Ni plating, respectively. The value before electroless Ni plating is higher but on the same order of magnitude as previously reported values of $0.0015 \, \Omega \cdot \text{cm}^2$ for Al on $0.5 \, \Omega \cdot \text{cm}$ p-type Si [18, 20, 21]. The increase in specific contact resistivity after electroless plating was due to spurious Ni plating at the Al-Si rear contacts [18]. Figure 2 shows an FIB image of Ni plated around a rear point contact on an IJP PERC cell that underwent electroless Ni plating. Nickel plates preferentially on the rear surface at regions where the Al is rough or contains a higher Si content than the surrounding Al [18]. In some areas, the Ni displaces the Al through galvanic displacement, coming into direct contact with the Si (see Figure 3). This plated Ni contributes to the metal Si contact and causes increased contact resistance due to the fact that Ni has a higher barrier height on p-type Si than Al [20].

The spurious rear-side Ni plating was only observed with cells and test structures which underwent electroless Ni plating. In bias-assisted LIP, the rear surface was protected from undesired plating by the bias voltage, and so rear-side plating was avoided. The absence of Ni on the rear contacts means that the Al-Si contact resistance measured from the test TLMs can be used as the contact resistance for rear contacts formed using BA-LIP.

3.2. Light IV Results. The cells were tested under standard conditions using an Adventest DC Voltage Current Source/Monitor, a temperature-controlled copper block, and a halogen lamp light source calibrated to one-sun using a calibrated reference cell. Suns-V_{oc} measurements were done using a flash tester, and the series resistance was estimated from comparing the light IV data to the Suns-V_{oc} data. The open-circuit voltage (V_{oc}), fill factor (FF), series resistance (R_s), and shunt resistance (R_{sh}) data for the cells plated using electroless Ni and BA-LIP Ni are listed in Table 3. The series resistance of the electroless Ni-plated cell was higher than that measured in the BA-LIP Ni-plated cell. The FFs of both cells are remarkably low. Shunting was an issue particularly for the BA-LIP sample, and the series resistance was high for both cells. The shunting in the BA-LIP batch of samples was due to inadequate resist coating on the front surface of the cell during the rear contact patterning step. Pinholes formed, creating holes through the dielectric and emitter which were subsequently plated with metal.

3.3. Photoluminescence Results. Photoluminescence imaging gives a spatially resolved image of locations of high and low voltages within a cell or wafer. When the cell is at open circuit, there is no lateral current flow, so areas of low voltage represent areas of high recombination. The PL intensity is directly proportional to the exponential of the voltage according to (1) [22]:

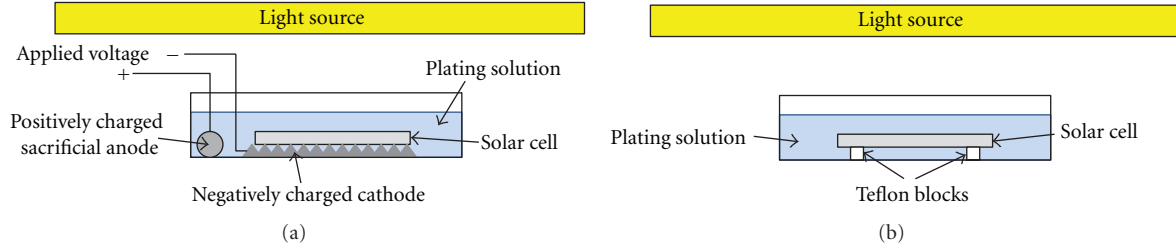$$I_{\text{PL},i} = C_i \exp\left(\frac{eU_i}{kT}\right), \tag{1}$$

FIGURE 1: Experimental setup for (a) bias-assisted LIP; (b) noncontact LIP.

TABLE 1: Processing sequence for IJP PERC cells.

Step	Process	Conditions
(1)	Damage etch/texture	20 min etch in 30% NaOH at 80°C
(2)	Oxidation	Dry oxidation, 1030°C for 4 hr with 1% TCA in O_2
(3)	Strip front oxide	Mask rear; strip SiO_2 with buffered HF
(4)	Emitter diffusion + oxidation	Diffusion: P solid source, 850°C, 15 min Oxidation: 1100°C, 5 hr, 1% TCA in O_2, 15 min anneal in N_2
(5)	IJP the front contacts	Indirect IJP method [5]
(6)	Groove diffusion + drive-in	Diffusion: P solid source, 940°C, 90 min Drive-in: 1000°C, 3 hr, N_2
(7)	IJP the rear contacts	Indirect IJP method [5]
(8)	Evaporate rear Al + sinter	1-2 μm Al, sinter at 400°C, 30 min in forming gas
(9)	Ni plate + anneal	Various plating methods; anneal at 400°C, 10 min in forming gas
(10)	Cu light-induced plate	Cu electroplating solution, 5 min under high-intensity fluorescent light
(11)	Edge isolation	Cut with a 1064 nm Nd : YAG laser from the rear; cut 1/2 way thru wafer then snapped

Ni plating was done in one of two ways: (i) electroless Ni using Transene EN solution [9], 80°C for 3 min; or (ii) BA-LIP Ni, 25–30°C for 30 s under high-intensity fluorescent light. The BA-LIP Ni consisted of Watt's solution in the ratios 10 g Ni_2SO_4, 20 g $NiCl_2$, 4 g boric acid in 100 mL deionized water [13]. The electroplating solution for the Cu plating used 12 g $CuSO_4$, 11 mL H_2SO_4, and 50 mL deionized water.

TABLE 2: Dimensions for cell design and analysis.

Parameter	Value	Variability
Cell area	8 cm^2	±0.15 cm^2
Finger width	90 μm	±10 μm
Finger height	5 μm	±2 μm
Finger length	28 mm	±0.5 mm
Finger spacing	1.2 mm	±10 μm
Rear contact diameter	100 μm	±10 μm
Rear contact spacing	1.5 mm	±10 μm

where $I_{PL,i}$ is the PL intensity at a specific location i, U_i is the voltage at that location, and C_i is a local calibration constant. With an open circuit PL image, the calibration constant can be calculated using the V_{oc} obtained from the light IV measurement along with the average PL signal from the PL image [22]. This then allows the voltage at any particular point in the image to be calculated from the PL signal.

Figure 4(a) shows an open-circuit PL image of an inkjet-patterned PERC cell that had its front metal contacts formed using electroless Ni plating followed by LIP Cu plating. The rear point contacts can be clearly seen in this image. At open circuit, with no current extraction occurring, locations of
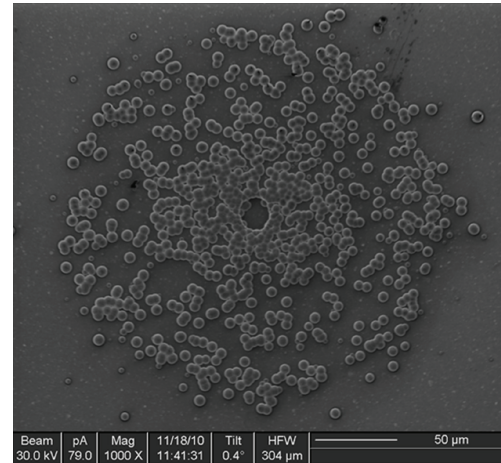

FIGURE 2: Focused ion beam (FIB) image of the rear of a test cell. Unwanted Ni plating can be seen around a rear point contact on an IJP PERC cell plated using electroless Ni [18].

low voltage must be due to either shunts or high recombination (low lifetime). Some shunts are apparent, as larger dark spots in a few locations on the wafer, but the regular

TABLE 3: Cell performance from light IV data.

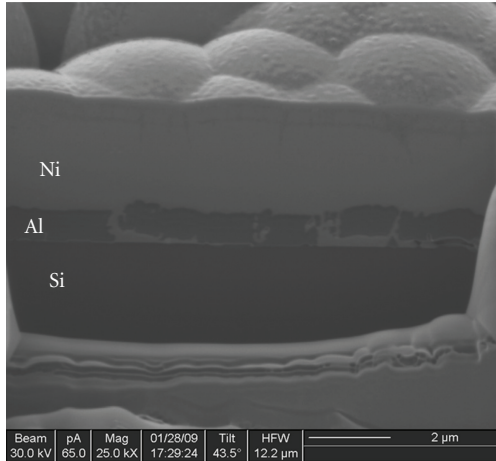| Ni-plating method	V_{oc} (mV)	Fill factor	Series resistance ($\Omega \cdot cm^2$)	Shunt resistance ($k\Omega \cdot cm^2$)
Electroless Ni	646	0.61	4.1	42.7
Bias-assisted LIP Ni	617	0.59	1.5	0.10

FIGURE 3: Focused ion beam (FIB) cross-section image of the rear contact of a test cell. Unwanted electroless Ni plating at the rear point contact has displaced some of the Al, contacting the Si surface and increasing the contact resistance [18].

rear contact design is also seen as a regular, shadowy pattern across the entire wafer. These contact locations are necessarily identified as locations of high recombination as a result.

Figure 4(b) shows the series resistance PL image of an electroless Ni-plated cell. In this image, bright areas indicate regions of high series resistance. Prominent features are the bright areas on the left and right edges of the cell, as well as the two darker regions spreading out from the busbar, again to the left and right sides of the cell. The bright regions on the very edges are regions of high series resistance caused by the edge cleave being too far away from the front contact grid. This can be easily corrected with more careful processing. The dark regions spreading out from the busbar indicate that the series resistance in these areas increases as you move away from the busbar—the resistance is limited by the line resistance of the fingers. In the centre, the whole area is orange (high resistance—about $6\,\Omega \cdot cm^2$) which is likely due to poor contact between the Ni and the Si, creating a high resistance everywhere. The average series resistance of this cell measured from the PL image data is $5.25\,\Omega \cdot cm^2$.

Figure 5(a) shows the open-circuit PL image for a cell fabricated using BA-LIP Ni and LIP Cu. The rear point contacts are no longer visible, indicating that the recombination at the contacts is less than it was for the electrolessly Ni-plated cells.

Figure 5(b) shows the series resistance PL image of the same BA-LIP Ni-plated cell. Due to both the decreased resistive losses at both the front and rear contacts, it was expected that the total R_s of bias-assisted LIP Ni cells would be less than the electroless Ni-plated cells, and this is in fact

the case. There are fewer bright regions on this sample, with an average series resistance of $2.9\,\Omega \cdot cm^2$ being measured using this method (IV measurements indicate $1.48\,\Omega \cdot cm^2$— the discrepancy between the measurements may be due to the low shunt resistance affecting the R_s calculation from the IV data). Some high resistance is again seen at the edge of the cell, due to the edge cleave again being too distant from the front contact grid. One finger peeled off the front, and this region of slightly higher series resistance is highlighted by the blue circle, but in general this image shows a much more uniform resistance across the surface of the cell. This means that the contact between the Ni and Si that is formed through BA-LIP Ni plating is more uniformly good across the surface of the wafer.

3.4. Breakdown Analysis of Series Resistance. Figure 6 depicts the sources of series resistance in a PERC cell. The lateral resistance through the emitter (1), line resistance through the fingers (3), resistance through the base (4), and spreading resistance at the rear contacts (5) are all functions of the material properties and geometry, and as such can be estimated from theory. The contact resistances, at (2) and (6), require measurements to be performed, as the actual resistance at contact locations is often very different to the theoretically expected resistance [23].

Table 4 summarizes the total estimated series resistance contribution based on the theoretical and experimental calculations, as well as the associated power loss from each type of series resistance. The percent power loss was calculated using (2). Effective resistances must be calculated in order to use this equation as, for example, not the full current generated flows through the full sheet resistance. Details on how to calculate the individual effective resistances are provided in the appendix:

$$\%P_{loss} = \frac{P_{loss}}{P_{gen}} = \frac{I_{MP}^2 R_{eff}}{I_{MP} V_{MP}} = \frac{I_{MP} R_{eff}}{V_{MP}}. \qquad (2)$$

As a percentage of total power loss, the rear point contacts are a major contributor to the overall series resistance on the electroless Ni-plated cells. For the cells Ni plated using BA-LIP, the calculated total resistance was within 1% of that estimated from the R_s-PL measurements. The value used for the rear contact resistance was that measured for an Al-Si contact after Ni plating; however, the FIB images show that there is also spurious Cu present at the rear contacts. As the calculated expected resistance is close to that measured, it is assumed that the spurious Cu did not have a significant impact on the series resistance of the finished devices.

For the cells where the Ni plating was achieved using electroless plating, the calculated total resistance is far greater than the resistance estimated from the IV measurements.
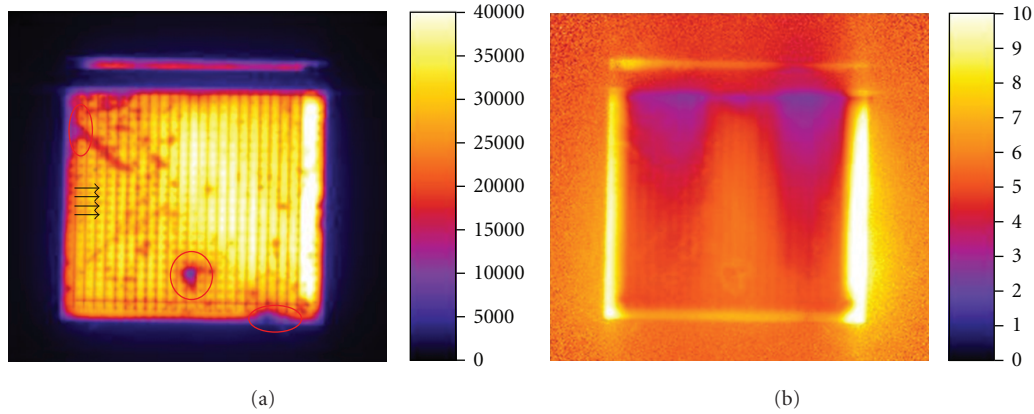
(a)

(b)

FIGURE 4: (a) Open-circuit PL image of a PERC cell made using EN and LIP Cu. The brighter the area, the higher the voltage in that location. The arrows highlight the locations of some of the rear point contacts, red circles are locations of shunts; (b) series resistance PL image of the same cell, bias voltage is -300 mV.
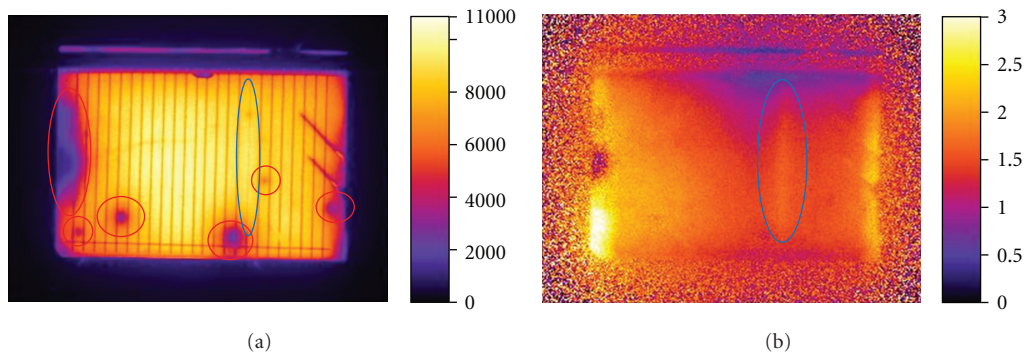

(a)

(b)

FIGURE 5: (a) Open-circuit PL image of a PERC cell fabricated using BA-LIP Ni and LIP Cu plating. The edges of the cell have been isolated with a laser. Red circles are shunt locations. Blue circle location of a peeled finger; (b) series resistance PL image of the same cell using a bias voltage of -300 mV.
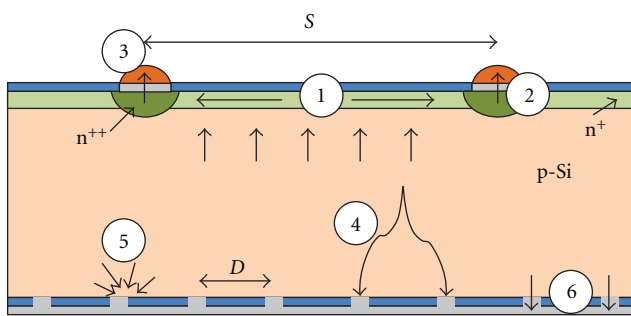

FIGURE 6: Locations of series resistance contributors in a PERC solar cell. S denotes the spacing between the front fingers, and D the spacing between the rear contact points. The length of the fingers is denoted by L (after [23]).

A worst-case scenario was used for the base contact resistance, as the variability in the contact resistance measurements can be great depending on how bad the spurious Ni on the rear is. Despite using the worst-case experimental values for ρ_c, the true value could be as low as $0.049\,\Omega\cdot\mathrm{cm}^2$ contribution, resulting in a percent power loss of 2.5%.

The variation across the electroless plated Ni cells is thought to be due to the variation in the severity of the excess Ni plating that occurs from cell to cell.

Focused ion beam (FIB) was used to examine the test cell contacts in order to track down a cause of the high resistance in the cells plated using BA-LIP. The rear contacts exhibited some unwanted plating once again, but this time from the LIP Cu. Figure 7 shows a cross-section of a rear contact from a cell plated using bias-assisted LIP.

Light-induced plating is an equivalent technique to electroplating, with the plating voltage being supplied by the cell itself. As such, it was expected that Cu plating would only occur on the front surface. Cu plated to the rear, though, again in the locations around the rear point contacts. This is thought to be caused by local areas of relatively different voltage. At the rear surface, the Al is oxidizing due to electrons being drained to the front of the cell and driving the reduction of Cu at the front surface. However, the first Al to oxidize will be the Al that is in direct contact with the Si surface. The electrons will be taken from there first, and a voltage potential will form between the Al in contact with the Si and the Al that is floating on the dielectric. The reduction of hydrogen at cathodic sites on the rear surface

TABLE 4: Sources of series resistance.

Resistance source	Electroless Ni		Bias-Assisted LIP Ni	
	R_s ($\Omega \cdot \text{cm}^2$)	P_{loss}(%)	R_s ($\Omega \cdot \text{cm}^2$)	P_{loss} (%)
Lateral resistance through the emitter	0.152	0.6	0.152	0.6
Line resistance along the fingers*	0.112	0.4	0.112	0.4
Resistance through the base*	0.072	0.3	0.072	0.3
Spreading resistance**	0.560	2.2	0.560	2.2
Front contact resistance	0.090	4.6	0.107	5.5
Rear contact resistance***	0.028	28.7	0.004	4.1
Total	**4.9**	**36.7**	**2.7**	**13.0**
Total measured R from IV	**4.1**		**1.48**	
Total measured R from R_s-PL	**5.3**		**2.9**	

* [14, 15].
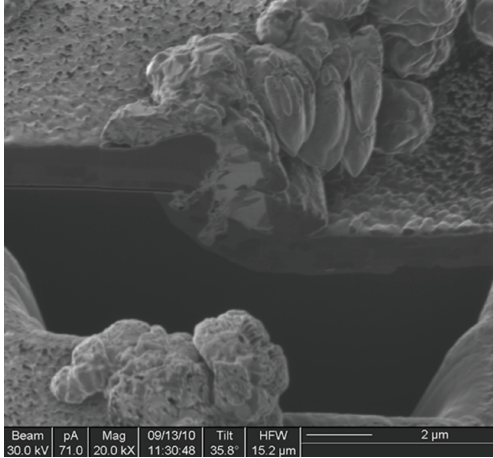** [16, 17].
*** From [18].

FIGURE 7: Focused ion beam (FIB) image of the rear of a BA-LIP Ni with LIP Cu test cell. Unwanted Cu plating can be seen at the edges of the rear point contacts.

can result in the formation of bubbles which can cause pitting and variations in surface potential [24]. Bias-assisted LIP of Cu where the rear surface is not in contact with the plating solution should address these issues. A number of commercial tool manufacturers are now developing BA-LIP tools which keep the Al rear surfaces of cells dry [25].

4. Summary and Future Research

In order to achieve higher-efficiency solar cells at lower cost, new fabrication methods such as inkjet patterning and metal plating may need to be considered. This research has identified and quantified the major series resistance losses inherent in the IJP PERC cell. The rear contact resistance of the Al-Si contacts is higher than expected for cells that were Ni plated using both electroless plating and BA-LIP. This results in higher series resistance and lower fill factors being achieved than is desirable. The specific contact resistivity of the these rear contacts in the electroless Ni-plated cells was an order of magnitude greater than for the cell plated using

BA-LIP due to spurious plating of Ni in the regions of the rear contacts.

Future work should focus on methods of achieving low resistance contacts on the rear of the cell. Bias-assisted LIP tools which maintain the rear surface dry will be required to ensure that plated metals do not interfere the electrical properties of the rear contacts. In addition to the rear contact resistance, the rear spreading resistance also needs to be reduced. Ideally this would be achieved by spacing the contacts closer together; however, unless the contact regions are heavily doped to minimize the minority carrier concentration at the surface, the recombination in the device will be increased resulting in a lower device voltage. Future work can also focus on how to form doped rear contact regions, either through laser-fired contacts [2], laser doping [1, 3], or local Al BSFs formed by firing Al through openings in a rear passivation layer.

Appendix

The locations where series resistance occurs in the cell are shown in Figure 5. In this section, the calculations done for determining each portion of the series resistance are shown.

(A) Lateral Resistance through the Emitter. When calculating the series resistance as a result of the current flowing through the emitter, it is important to note that not all the current will see the full resistance; the current generated close to the contact fingers will have less distance to travel through the emitter and experience less resistance than current generated midway between two fingers. A proper summation of the current must be done in order to obtain the effective resistance contribution from the emitter. From [14, 15], the following equation can be used to determine the resistance contribution from the emitter:

$$R_{\text{eff}} = \frac{1}{3} \frac{S/2}{L} \frac{\rho}{t}, \qquad (A.1)$$

where S is the finger spacing, L is the length of the fingers, and ρ/t is the sheet resistance of the emitter. With an emitter sheet resistance of ~120 Ω/sq, the effective resistance

contribution of the emitter is calculated to be 0.019 Ω. As the dimensions on all the test cells are the same, this is the expected contribution on all the wafers.

(B) Line Resistance along the Fingers. As with the emitter, not all the current flows through the full length of the fingers; the current generated close to the busbar will have less distance to travel through the metal than the current generated on the far side of the cell. As such, the geometry of the problem is the same, and the same equation that was used to calculate the effective series resistance for the emitter can be used for the fingers. In this case,

$$R_{\text{eff}} = \frac{1}{3} \frac{L}{W} \frac{\rho}{t}, \tag{A.2}$$

where L is again the length of the fingers, W is the width of the fingers, ρ is the specific resistivity of the Cu, and t is the thickness of the Cu. From the dimensions and the resistivity of Cu being 16.78 nΩ·m, the effective resistance from the front fingers works out to be 0.014 Ω.

(C) Resistance through the Base. The resistance contribution from the base can be calculated from:

$$R_b = \rho_b D, \tag{A.3}$$

where ρ_b is the resistivity of the base and D is the spacing between the rear contacts [16]. From the geometry and a base resistivity of 0.5 Ω·cm, the resistance through the base material is 0.075 Ω·cm^2, and a total resistance contribution of 9.4 mΩ.

(D) Spreading Resistance at the Rear Contacts. The spreading resistance at the base point contacts can be calculated from the geometry and the material properties of Si from:

$$R_{\text{sp}} = D^2 \frac{\rho_b}{2d_c}, \tag{A.4}$$

where ρ_b is the resistivity of the base, D is the spacing of the rear contacts, and d_c is the diameter of the rear contact [15, 16]. From the geometry and a base resistivity of 0.5 Ω·cm, the spreading resistance at the rear contacts works out to be 0.56 Ω·cm^2, and a total resistance of 0.07 Ω.

(E) Contact Resistance. Contact resistance between the metal contacts and the Si was determined from TLM test structures, the details of which were given in Sections 3.1 and 3.4.

Acknowledgment

References

[1] Suntech Power Co. Ltd., http://www.suntech-power.com/.

[2] E. Schneiderlochner, R. Preu, R. Ldemann, and S. W. Glunz, "Laser-fired rear contacts for crystalline silicon solar cells," *Progress in Photovoltaics: Research and Applications*, vol. 10, no. 1, pp. 29–34, 2002.

[3] B. S. Tjahjono, L. Mai, Z. Hameiri et al., "High efficiency solar cell structures through the use of laser doping," in *Proceedings of the 22nd European Photovoltaic Solar Energy Conference*, pp. 966–969, Milan, Italy, 2007.

[4] R. Y. Utama, A. J. Lennon, M. A. Lenio et al., "Inkjet printing for high efficiency selective emitter silicon solar cells," in *Proceedings of the 22nd European Photovoltaic Solar Energy Conference*, pp. 1687–1690, Valencia, Spain, 2008.

[5] A. J. Lennon, R. Y. Utama, M. A. T. Lenio, A. W. Y. Ho-Baillie, N. B. Kuepper, and S. R. Wenham, "Forming openings to semiconductor layers of silicon solar cells by inkjet printing," *Solar Energy Materials and Solar Cells*, vol. 92, no. 11, pp. 1410–1415, 2008.

[6] T. Bruton, N. Mason, S. Roberts et al., "Towards 20% efficient silicon solar cells manufactured at 60 MWp per annum," in *Proceddings of the 3rd World Conference on Photovoltaic Energy Conversion*, pp. 899–902, Osaka, Japan, May 2003.

[7] A. Wang, *High efficiency PERC and PERL silicon solar cells [Ph.D. thesis]*, Department of Electrical Engineering, University of New South Wales, Sydney, Australia, 1992.

[8] M. Lenio, J. Howard, F. Jentschke, A. Lennon, and S. Wenham, "Design, fabrication and analysis of high efficiency inkjet printed passivated emitter rear contacted solar cells," in *Proceedings of the 37th IEEE Photovoltaic Specialists Conferenc (PVSC '11)*, Seattle, Wash, USA, 2011.

[9] M. Aleman, N. Bay, M. Fabritius, and S. Glunz, "Characterization of electroless nickel plating on silicon solar cells for the front side metallization," in *Proceedings of the 22nd European Photovoltaic Solar Energy Conference*, pp. 1590–1592, Milan, Italy, 2007.

[10] D. Pysch, A. Mette, and S. W. Glunz, "A review and comparison of different methods to determine the series resistance of solar cells," *Solar Energy Materials and Solar Cells*, vol. 91, no. 18, pp. 1698–1706, 2007.

[11] T. Trupke, E. Pink, R. A. Bardos, and M. D. Abbott, "Spatially resolved series resistance of silicon solar cells obtained from luminescence imaging," *Applied Physics Letters*, vol. 90, no. 9, Article ID 093506, 3 pages, 2007.

[12] H. Kampwerth, T. Trupke, J. W. Weber, and Y. Augarten, "Advanced luminescence based effective series resistance imaging of silicon solar cells," *Applied Physics Letters*, vol. 93, no. 20, Article ID 202102, 3 pages, 2008.

[13] Transene Company Inc., http://www.transene.com/.

[14] N. C. Wyeth, "Sheet resistance component of series resistance in a solar cell as a function of grid geometry," *Solid State Electronics*, vol. 20, no. 7, pp. 629–634, 1977.

[15] L. D. Nielsen, "Distributed series resistance effects in solar cells," *IEEE Transactions on Electron Devices*, vol. 29, no. 5, pp. 821–827, 1982.

[16] J. Zhao, A. Wang, and M. A. Green, "Series resistance caused by the localized rear contact in high efficiency silicon solar cells," *Solar Energy Materials and Solar Cells*, vol. 32, no. 1, pp. 89–94, 1994.

[17] B. Gelmont and M. Shur, "Spreading resistance of a round ohmic contact," *Solid-State Electronics*, vol. 36, no. 2, pp. 143–146, 1993.

[18] M. A. T. Lenio, A. J. Lennon, A. Ho-Baillie, and S. R. Wenham, "Effect of electroless nickel on the series resistance of high-efficiency inkjet printed passivated emitter rear contacted solar cells," *Solar Energy Materials and Solar Cells*, vol. 94, no. 12, pp. 2102–2107, 2010.

[19] E. J. Lee, D. S. Kim, and S. H. Lee, "Ni/Cu metallization for low-cost high-efficiency PERC cells," *Solar Energy Materials and Solar Cells*, vol. 74, no. 1–4, pp. 65–70, 2002.

[20] S. Sze and K. K. Ng, *Physics of Semiconductor Devices*, John Wiley & Sons, New Jersey, NJ, USA, 3rd edition, 2007.

[21] K. K. Ng and R. Liu, "On the calculation of specific contact resistivity on <100> silicon," *IEEE Transactions on Electron Devices*, vol. 37, pp. 1535–1537, 1990.

[22] P. Wurfel, *Physics of Solar Cells*, vol. 1, Wiley-VCH, Weinheim, Germany, 2005.

[23] A. Milne, *The passivated emitter and rear solar cell [Ph.D. thesis]*, Department of Electrical Engineering, University of New South Wales, Sydney, Australia, 1991.

[24] G. A. DiBari, "Nickel plating," *Metal Finishing*, vol. 93, no. 1, pp. 259–279, 1995.

[25] Technic Inc., "SEMCON semiconductor plating tools," http://www.technic.com/.

Journal of
Nanotechnology

International Journal of
Corrosion

International Journal of
Polymer Science

Smart Materials
Research

Journal of
Composites

BioMed
Research International

Journal of
Materials

Journal of
Metallurgy

Hindawi

Submit your manuscripts at
http://www.hindawi.com

Journal of
Nanoparticles

Advances in
Materials Science and Engineering

Scientifica

Journal of
Nanomaterials

The Scientific
World Journal

International Journal of
Biomaterials

Journal of
Nanoscience

Journal of
Coatings

Journal of
Crystallography

Journal of
Ceramics

Journal of
Textiles